Model-based Sensorless Control of IPMSM Enhancing Robustness based on the Estimation of Speed Error

Younggi Lee and Seung-Ki Sul
Department of Electrical and Computer Engineering
Seoul National University
Seoul, Korea
younglee@eepel.snu.ac.kr, sulsk@plaza.snu.ac.kr

Abstract— **In this paper, new model-based sensorless control methods are proposed, including estimation methods for the position and speed errors and compatible position and speed estimators. In proposed methods, the speed error is estimated as well as the position error in the conventional model-based sensorless methods. By the proposed methods, unity transfer function from actual position to estimated position can be achieved eliminating the effects of load disturbances. It means that the position error would be ideally zero even in transient situations. Experimental results verify the effectiveness of the proposed methods under severe speed transient (20,000 r/min/s) and load torque transient (20 p.u./s). With the proposed methods, position error has been conspicuously reduced by 60% at speed transient and by 70% at load torque transient in high speed region.**

Keywords—IPMSM; model-based sensorless; sensorless control; robustness; speed error;

I. INTRODUCTION

Sensorless control of Interior Permanent Magnet Synchronous Machine (IPMSM) has been widely used in various drive applications including home appliances and traction systems. Since the merits such as cost, volume, and reliability can be achieved by sensorless control, many approaches to estimate the rotor position and speed have been developed for a few decades [1-15]. In sensorless control, generally, they can be divided into two categories: high-frequency signal injection methods (HFSIM) [1-5] and model-based methods (MBM) [6-15]. The former is based on the magnetic saliency in high-frequency range and used in standstill and low speed region. However, since the operating speed is limited and the additional loss is imposed due to the injection voltage, the latter is preferred in higher speed region.

In both methods, i.e., HFSIM, and MBM, accurate estimation performance and increased control bandwidth have been important issues. Regarding the accurate estimation of the rotor position, it has been disclosed that the distorted voltage by inverter should be compensated in both methods [2, 6-8]. In these researches, it was shown that the distortion from the reference voltage is related with the resulting position error. Also, it was turned out that the cross-coupling and non-linearly varying inductances have an effect on the position error and they were considered in the signal-processing procedures [3]. More precise machine model using Extended Electromotive force (EEMF) concept [9-10], online parameter identification scheme [6] and representative parameter selection minimizing the position error [11] were proposed to achieve the accurate position estimation performance.

Meanwhile, for the increased control bandwidth, position and speed estimator including mechanical equation was proposed [12]. In [12], by employing the torque feed-forward into the estimator, phase lagging property in the estimation was eliminated. This scheme can be also applied to HFSIM in same manner. Especially, in HFSIM, there were attempts for higher control bandwidth by increasing the injection frequency until switching frequency which is the theoretical limitation [4-5]. They enable that the overall bandwidth of the system including position, speed and current control can be extended.

Despite of continuous efforts to enhance the performance, still the sensorless control is vulnerable to load disturbances. Even if a robustness in the position estimation is one of the most important characteristics in actual application, since the load disturbance is not predictable, it has remained as a weak point in both sensorless methods, i.e., HFSIM and MBM. Naturally, there were several approaches to increase robustness of the system against the load disturbance such as disturbance torque observer [13]. However, inherently, the bandwidth of the disturbance observer is limited according to the system and, therefore, it is not suitable in the most of servo application.

Therefore, in this paper, new model-based sensorless control methods are proposed, including estimation methods for the position and speed errors and compatible position and speed estimators. In the proposed methods, the speed error is estimated as well as the position error in the conventional MBMs. Though the classical papers covered the sensorless methods using the speed error information [14-15], their concept for the speed error is different with this paper and, for this reason, several terms which are important in high speed operation were neglected in previous researches. In the proposed methods, meanwhile, unity transfer function from actual position to estimated position can be achieved eliminating the effects of load disturbances. It means that the position error would be ideally zero even in transient situations. Experimental results verify the effectiveness of the proposed methods under severe speed transient (20,000 r/min/s) and load torque transient (20 p.u./s). With the proposed methods, position error has been conspicuously reduced by 60% at speed transient and by 70% at load torque transient in high speed region.

II. Conventional Model-based Sensorless Control

In medium- and high-speed regions, the rotor position and speed are estimated by MBM since the additional voltage injection is not required and, therefore, loss can be reduced. In this chapter, conventional methods would be introduced. One is the MBM using an EEMF concept and the other is the sensorless methods using a speed error which is considered as a differentiation of the position error.

The fundamental model of PMSM in rotor reference frame where d-axis is placed toward the rotor position (= θ_r) is given by (1).

$$\begin{bmatrix} v_{ds}^r \\ v_{qs}^r \end{bmatrix} = \begin{bmatrix} R_s & -\omega_r L_{qs} \\ \omega_r L_{ds} & R_s \end{bmatrix} \begin{bmatrix} i_{ds}^r \\ i_{qs}^r \end{bmatrix} + \begin{bmatrix} L_{ds} & 0 \\ 0 & L_{qs} \end{bmatrix} \frac{d}{dt} \begin{bmatrix} i_{ds}^r \\ i_{qs}^r \end{bmatrix} + \begin{bmatrix} 0 \\ \omega_r \lambda_f \end{bmatrix}, \quad (1)$$

where v_{ds}^r , v_{qs}^r , i_{ds}^r , i_{qs}^r , and L_{ds}, L_{qs} stand for the d- and q-axes voltages, currents and static inductances respectively. Additionally, R_s for the stator-winding resistance, λ_f for the flux linkage from permanent magnets, ω_r for the rotational speed in electrical angle. In (1), it is assumed that the effects of coupling inductances such as L_{dqs} and L_{qds} are sufficiently small.

In sensorless control, however, every control methods are carried out in the estimated rotor reference frame. Thus, Eq. (1) in the rotor reference frame should be expressed in the estimated frame. Then, it can be noticed from (2) that the complicated terms are induced since the inductance and coupling matrices are asymmetric due to the saliency. In (2), $\tilde{\theta}_r$ is defined as a position error between the real rotor position and the estimated one, i.e., $\theta_r - \hat{\theta}_r$ and the symbol '^' in superscript means the variable represented in the estimated frame. To simplify the mathematical expression in the estimated frame, (1) can be rearranged as (3) with the introduction of EEMF concept, i.e., E_{ex}.

$$\begin{bmatrix} v_{ds}^r \\ v_{qs}^r \end{bmatrix} = \begin{bmatrix} R_s & -\omega_r L_{qs} \\ \omega_r L_{qs} & R_s \end{bmatrix} \begin{bmatrix} i_{ds}^r \\ i_{qs}^r \end{bmatrix} + \begin{bmatrix} L_{ds} & 0 \\ 0 & L_{ds} \end{bmatrix} \frac{d}{dt} \begin{bmatrix} i_{ds}^r \\ i_{qs}^r \end{bmatrix} + \begin{bmatrix} 0 \\ E_{ex} \end{bmatrix}, \quad (3)$$

where $E_{ex} \equiv \omega_r \lambda_f + \omega_r L_\Delta i_{ds}^r - L_\Delta \frac{d}{dt} i_{qs}^r$ and $L_\Delta \equiv L_{ds} - L_{qs}$. Then, voltage equation of IPMSM can be expressed as if inductance matrices were symmetric. Similarly, Eq. (3) can be expressed in the estimated frame as (4).

$$\begin{bmatrix} v_{ds}^{\hat{r}} \\ v_{qs}^{\hat{r}} \end{bmatrix} = \begin{bmatrix} R_s & -\omega_r L_{qs} \\ \omega_r L_{qs} & R_s \end{bmatrix} \begin{bmatrix} i_{ds}^{\hat{r}} \\ i_{qs}^{\hat{r}} \end{bmatrix} + \begin{bmatrix} L_{ds} & 0 \\ 0 & L_{ds} \end{bmatrix} \frac{d}{dt} \begin{bmatrix} i_{ds}^{\hat{r}} \\ i_{qs}^{\hat{r}} \end{bmatrix} + \begin{bmatrix} e_{ds}^{\hat{r}} \\ e_{qs}^{\hat{r}} \end{bmatrix}, \quad (4)$$

$$\text{where } \begin{bmatrix} e_{ds}^{\hat{r}} \\ e_{qs}^{\hat{r}} \end{bmatrix} = E_{ex} \begin{bmatrix} -\sin\tilde{\theta}_r \\ \cos\tilde{\theta}_r \end{bmatrix} + (\omega_r - \hat{\omega}_r) L_{ds} \begin{bmatrix} i_{qs}^{\hat{r}} \\ -i_{ds}^{\hat{r}} \end{bmatrix}.$$

Based on (4), various type of estimators for EEMF were proposed under the assumption of $\tilde{\omega}_r \equiv \omega_r - \hat{\omega}_r = 0$. One of the classical estimators is shown in Fig. 1. In Fig. 1, parameters

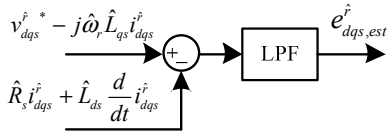

Fig. 1. Conventional extended EMF estimator.

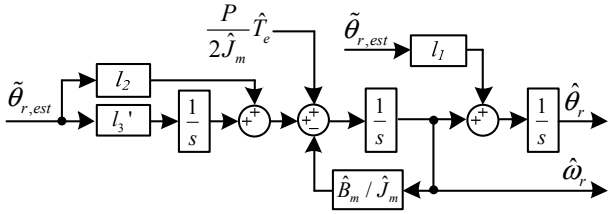

Fig. 2. Conventional position and speed estimator.

with '*est*' in the subscript mean the estimated ones. The output of the estimator, i.e., $e_{dqs,est}^{\hat{r}}$, is used as an input of position and speed estimator after simple signal processing of (5).

$$\tilde{\theta}_{r,est} = \tan^{-1}\left(-\frac{e_{ds}^{\hat{r}}}{e_{qs}^{\hat{r}}}\right) \text{ or } -\frac{e_{ds}^{\hat{r}}}{\hat{E}_{ex}}. \quad (5)$$

For the estimation of position and speed, PID type position and speed estimator including torque feed-forward in Fig. 2 is commonly used [2, 12]. In Fig. 2, P indicates the number of poles. Then, the estimator in Fig. 2 adjusts the estimated position, $\hat{\theta}_r$, and speed, $\hat{\omega}_r$, without phase delay in the direction that $\tilde{\theta}_{r,est}$ would be nullified.

On the other hand, as aforementioned in introduction, several classical papers had covered the sensorless methods using a speed or EMF error for non-salient machines (L_s=L_{ds}=L_{qs}) [14-15]. In these papers, the position and speed (or EMF) errors were estimated based on the difference between measured and estimated current variation based on (1). Eq. (6) shows the exact expression of the difference.

$$\begin{bmatrix} \Delta i_{ds}^{\hat{r}} \\ \Delta i_{qs}^{\hat{r}} \end{bmatrix} - \begin{bmatrix} \Delta i_{ds,est}^{\hat{r}} \\ \Delta i_{qs,est}^{\hat{r}} \end{bmatrix} = \frac{T_{samp}}{L_s} \left(\begin{array}{l} \lambda_f \begin{bmatrix} \omega_r \sin\tilde{\theta}_r \\ \hat{\omega}_r - \omega_r \cos\tilde{\theta}_r \end{bmatrix} \\ + L_s \frac{d}{dt}\tilde{\theta}_r \begin{bmatrix} 0 & -1 \\ 1 & 0 \end{bmatrix} \begin{bmatrix} i_{ds}^{\hat{r}} \\ i_{qs}^{\hat{r}} \end{bmatrix} \\ + L_s \begin{bmatrix} 0 & -\hat{\omega}_r + \omega_r \\ \hat{\omega}_r - \omega_r & 0 \end{bmatrix} \begin{bmatrix} i_{ds}^{\hat{r}} \\ i_{qs}^{\hat{r}} \end{bmatrix} \end{array} \right). \quad (6)$$

In this equation, it is assumed that $\hat{R}_s = R_s$, $\hat{L}_s = L_s$, and no voltage distortion by inverter. However, despite of these assumptions, previous researches had estimated the position and speed errors neglecting last two terms in (6). This is

$$\begin{bmatrix} v_{ds}^{\hat{r}} \\ v_{qs}^{\hat{r}} \end{bmatrix} = R_s \begin{bmatrix} i_{ds}^{\hat{r}} \\ i_{qs}^{\hat{r}} \end{bmatrix} + \begin{bmatrix} L_{ds}\cos^2\tilde{\theta}_r + L_{qs}\sin^2\tilde{\theta}_r & (L_{ds} - L_{qs})\sin\tilde{\theta}_r\cos\tilde{\theta}_r \\ (L_{ds} - L_{qs})\sin\tilde{\theta}_r\cos\tilde{\theta}_r & L_{ds}\sin^2\tilde{\theta}_r + L_{qs}\cos^2\tilde{\theta}_r \end{bmatrix} \frac{d}{dt} \begin{bmatrix} i_{ds}^{\hat{r}} \\ i_{qs}^{\hat{r}} \end{bmatrix} + \omega_r \lambda_f \begin{bmatrix} -\sin\tilde{\theta}_r \\ \cos\tilde{\theta}_r \end{bmatrix}$$
$$+ \frac{d}{dt}\tilde{\theta}_r \begin{bmatrix} -(L_{ds} - L_{qs})\sin\tilde{\theta}_r\cos\tilde{\theta}_r & L_{ds}\cos^2\tilde{\theta}_r + L_{qs}\sin^2\tilde{\theta}_r \\ -L_{ds}\sin^2\tilde{\theta}_r - L_{qs}\cos^2\tilde{\theta}_r & (L_{ds} - L_{qs})\sin\tilde{\theta}_r\cos\tilde{\theta}_r \end{bmatrix} \begin{bmatrix} i_{ds}^{\hat{r}} \\ i_{qs}^{\hat{r}} \end{bmatrix} + \omega_r \begin{bmatrix} -(L_{ds} - L_{qs})\sin\tilde{\theta}_r\cos\tilde{\theta}_r & -L_{ds}\sin^2\tilde{\theta}_r - L_{qs}\cos^2\tilde{\theta}_r \\ L_{ds}\cos^2\tilde{\theta}_r + L_{qs}\sin^2\tilde{\theta}_r & (L_{ds} - L_{qs})\sin\tilde{\theta}_r\cos\tilde{\theta}_r \end{bmatrix} \begin{bmatrix} i_{ds}^{\hat{r}} \\ i_{qs}^{\hat{r}} \end{bmatrix}. \quad (2)$$

because that the last two terms are almost cancelled out with each other and they cannot be seen in the difference of current variation. Therefore, extracted position and speed error from this method would not match with real ones in the case that the estimated speed becomes much different from real one, e.g., abrupt speed variation or load disturbances.

III. Proposed Sensorless Control Methods

A. Estimation of position and speed error

In proposed methods, position and speed errors are estimated based on (7). Eq. (7) has been simplified from (2) under the assumptions of $\sin\tilde{\theta}_r \approx \tilde{\theta}_r$, $\sin^2\tilde{\theta}_r \approx 0$ and $\cos\tilde{\theta}_r \approx 1$.

After simplification, since the actual speed cannot be obtained, it is segregated into the estimated speed and the speed error terms, i.e., $\omega_r = \hat{\omega}_r + \tilde{\omega}_r$, and rearranged as (8). This is the most important expression in this paper. Then, $\tilde{e}^{\hat{r}}_{ds}$ and $\tilde{e}^{\hat{r}}_{qs}$ terms defined as EMF errors can be estimated by known parameters since the actual speed or position is never required in (8). As the EMF errors contain the position and speed errors, they can be extracted from $\tilde{e}^{\hat{r}}_{dqs}$ and utilized for improved sensorless control. In $\tilde{e}^{\hat{r}}_{dqs}$, however, since the differential terms such as $d\tilde{\theta}_r/dt$ and $d\tilde{\theta}_r^2/dt$ are included, stability and dynamic characteristics should be considered in back calculation from $\tilde{e}^{\hat{r}}_{dqs}$ to $\tilde{\theta}_r$ and $\tilde{\omega}_r$. Moreover, design process for estimator considering stability and dynamics would be quite a complicated work because $\tilde{e}^{\hat{r}}_{dqs}$ is affected by variable parameters, such as ω_r and $i^{\hat{r}}_{dqs}$. However, $d\tilde{\theta}_r/dt$ and $d\tilde{\theta}_r^2/dt$ terms in (8) have negligible effects on $\tilde{e}^{\hat{r}}_{dqs}$, and they can be ignored as in (9).

$$\begin{bmatrix}\tilde{\omega}_{r,est}\\ \tilde{\theta}_{r,est}\end{bmatrix} = \frac{1}{c_{\omega,d}c_{\theta,q} - c_{\theta,d}c_{\omega,q}}\begin{bmatrix}c_{\theta,q} & -c_{\theta,d}\\ -c_{\omega,q} & c_{\omega,d}\end{bmatrix}\begin{bmatrix}\tilde{e}^{\hat{r}}_{ds}\\ \tilde{e}^{\hat{r}}_{qs}\end{bmatrix}. \quad (9)$$

B. Design of position and speed estimator

For the proposed estimation method for $\tilde{\theta}_{r,est}$ and $\tilde{\omega}_{r,est}$ simultaneously, conventional position and speed estimators such as Fig. 2 would not be suitable because they use only one input, i.e., $\tilde{\theta}_{r,est}$. However, in the proposed method, $\tilde{\omega}_{r,est}$ should be applied as well as $\tilde{\theta}_{r,est}$. Therefore, in this paper, new position and speed estimator exploiting the estimated errors in (9) is proposed as well. For the design of the estimator, state equation of (10) is used, and its structure is shown in Fig.3. In this figure,

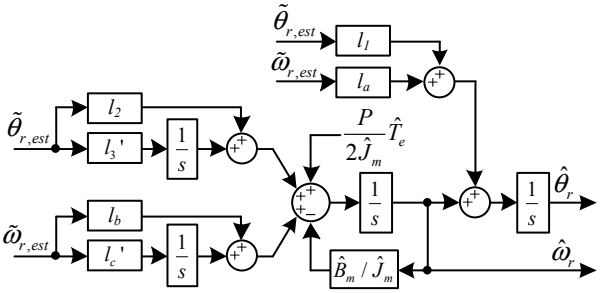

Fig. 3. Proposed position and speed estimator.

l_3' and l_c' indicate $-Pl_3/2\hat{J}_m$ and $-Pl_c/2\hat{J}_m$, respectively.

$$\frac{d}{dt}\begin{bmatrix}\hat{\theta}_r\\ \hat{\omega}_r\\ \hat{T}_L\end{bmatrix} = \begin{bmatrix}0 & 1 & 0\\ 0 & -\frac{\hat{B}}{\hat{J}_m} & -\frac{P}{2\hat{J}_m}\\ 0 & 0 & 0\end{bmatrix}\begin{bmatrix}\hat{\theta}_r\\ \hat{\omega}_r\\ \hat{T}_L\end{bmatrix} + \begin{bmatrix}0\\ \frac{P}{2\hat{J}_m}\\ 0\end{bmatrix}T_e + \begin{bmatrix}l_1 & l_a\\ l_2 & l_b\\ l_3 & l_c\end{bmatrix}\begin{bmatrix}\tilde{\theta}_{r,est}\\ \tilde{\omega}_{r,est}\end{bmatrix}. \quad (10)$$

As shown in (10) and Fig. 3, inputs of estimator are $\tilde{\theta}_{r,est}$ and $\tilde{\omega}_{r,est}$ from (9), and $\hat{\theta}_r$ and $\hat{\omega}_r$ are adjusted in the direction that both of inputs are nullified. Now, gain matrix in (10) should be determined. If the extracted errors are estimated well, that is, $\tilde{\theta}_{r,est}$ and $\tilde{\omega}_{r,est}$ are same with $\theta_r - \hat{\theta}_r$ and $\omega_r - \hat{\omega}_r$, respectively, then the gain matrix can be set according to the desired dynamic characteristics of the estimator. In (11) at next page, transfer functions from θ_r, ω_r, and ΔT to $\hat{\theta}_r$ and $\hat{\omega}_r$ are listed. In calculations for (11), $\tilde{\theta}_{r,est} = \tilde{\theta}_r$ and $\tilde{\omega}_{r,est} = \tilde{\omega}_r$ are assumed. Also, ΔT is defined as a disturbance torque which is the difference between the feed-forward input, $\hat{T}_e$, and net torque applied to the motor, i.e., $T_e - T_L$. Since they show the dynamic characteristics of the estimator, gain matrix is determined in order that each transfer function in (11) have the required characteristics.

In addition, it can be noticed from (11) that l_a=1 can completely eliminate the effect of ΔT on $\hat{\theta}_r$ even if the effect on $\hat{\omega}_r$ remains yet. Also, from l_a=1 and the relation of θ_r and ω_r, Eq. (12) can be deduced.

$$\begin{aligned}\hat{\theta}_r &= \left\{H_{\theta\theta}(s) + sH_{\theta\omega}(s)\right\}\theta_r = \theta_r,\\ \hat{\omega}_r &= \left\{\frac{1}{s}H_{\omega\theta}(s) + H_{\omega\omega}(s)\right\}\omega_r + H_{\omega T}(s)\Delta T = \omega_r + H_{\omega T}(s)\Delta T.\end{aligned} \quad (12)$$

$$\begin{bmatrix}v^{\hat{r}}_{ds}\\ v^{\hat{r}}_{qs}\end{bmatrix} = \begin{bmatrix}R_s & -\omega_r L_{qs}\\ \omega_r L_{ds} & R_s\end{bmatrix}\begin{bmatrix}i^{\hat{r}}_{ds}\\ i^{\hat{r}}_{qs}\end{bmatrix} + \begin{bmatrix}L_{ds} & 0\\ 0 & L_{qs}\end{bmatrix}\frac{d}{dt}\begin{bmatrix}i^{\hat{r}}_{ds}\\ i^{\hat{r}}_{qs}\end{bmatrix} + \begin{bmatrix}0\\ \omega_r\lambda_f\end{bmatrix} + \tilde{\theta}_r\begin{bmatrix}-\omega_r\lambda_f - \omega_r L_\Delta i^{\hat{r}}_{ds} + L_\Delta\frac{d}{dt}i^{\hat{r}}_{qs}\\ \omega_r L_\Delta i^{\hat{r}}_{qs} + L_\Delta\frac{d}{dt}i^{\hat{r}}_{ds}\end{bmatrix} + \frac{d}{dt}\tilde{\theta}_r\begin{bmatrix}L_{ds}i^{\hat{r}}_{qs}\\ -L_{qs}i^{\hat{r}}_{ds}\end{bmatrix} + \frac{1}{2}\frac{d}{dt}\tilde{\theta}_r^2\begin{bmatrix}-L_\Delta i^{\hat{r}}_{ds}\\ L_\Delta i^{\hat{r}}_{qs}\end{bmatrix}. \quad (7)$$

$$\begin{bmatrix}v^{\hat{r}}_{ds}\\ v^{\hat{r}}_{qs}\end{bmatrix} = \begin{bmatrix}R_s & -\hat{\omega}_r L_{qs}\\ \hat{\omega}_r L_{ds} & R_s\end{bmatrix}\begin{bmatrix}i^{\hat{r}}_{ds}\\ i^{\hat{r}}_{qs}\end{bmatrix} + \begin{bmatrix}L_{ds} & 0\\ 0 & L_{qs}\end{bmatrix}\frac{d}{dt}\begin{bmatrix}i^{\hat{r}}_{ds}\\ i^{\hat{r}}_{qs}\end{bmatrix} + \begin{bmatrix}0\\ \hat{\omega}_r\lambda_f\end{bmatrix} + \begin{bmatrix}\tilde{e}^{\hat{r}}_{ds}\\ \tilde{e}^{\hat{r}}_{qs}\end{bmatrix}, \quad (8)$$

where $\begin{bmatrix}\tilde{e}^{\hat{r}}_{ds}\\ \tilde{e}^{\hat{r}}_{qs}\end{bmatrix} = \tilde{\omega}_r\begin{bmatrix}-L_{qs}i^{\hat{r}}_{qs}\\ L_{ds}i^{\hat{r}}_{ds} + \lambda_f\end{bmatrix} + \tilde{\theta}_r\begin{bmatrix}L_\Delta\frac{d}{dt}i^{\hat{r}}_{qs} - \omega_r\lambda_f - \omega_r L_\Delta i^{\hat{r}}_{ds}\\ L_\Delta\frac{d}{dt}i^{\hat{r}}_{ds} + \omega_r L_\Delta i^{\hat{r}}_{qs}\end{bmatrix} + \frac{d}{dt}\tilde{\theta}_r\begin{bmatrix}L_{ds}i^{\hat{r}}_{qs}\\ -L_{qs}i^{\hat{r}}_{ds}\end{bmatrix} + \frac{1}{2}\frac{d}{dt}\tilde{\theta}_r^2\begin{bmatrix}-L_\Delta i^{\hat{r}}_{ds}\\ L_\Delta i^{\hat{r}}_{qs}\end{bmatrix} = \tilde{\omega}_r\begin{bmatrix}c_{\omega,d}\\ c_{\omega,q}\end{bmatrix} + \tilde{\theta}_r\begin{bmatrix}c_{\theta,d}\\ c_{\theta,q}\end{bmatrix} + \frac{d}{dt}\tilde{\theta}_r\begin{bmatrix}c_{\theta1,d}\\ c_{\theta1,q}\end{bmatrix} + \frac{d}{dt}\tilde{\theta}_r^2\begin{bmatrix}c_{\theta2,d}\\ c_{\theta2,q}\end{bmatrix}$.

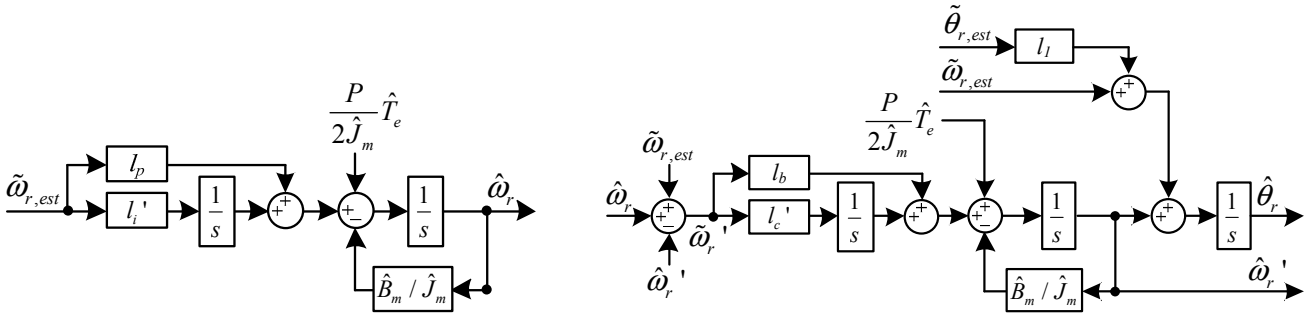

(a) Auxiliary speed estimator

(b) Modified position estimator

Fig. 4. Modified position and speed estimator including the proposed auxiliary speed estimator.

In (12), it can be noted that $\hat{\theta}_r$ have the perfect robustness against the speed or load torque variation since $H_{\theta\theta}(s)+sH_{\theta\omega}(s)$ and $H_{\theta T}(s)$ are unity and null, respectively, regardless of the accuracy of the estimation of mechanical parameters. Also, $H_{\omega\theta}(s)/s+H_{\omega\omega}(s)$ in (12) becomes unity. However, in this case, the estimated mechanical parameter, $\hat{J}_m$ and $\hat{B}_m$ should be identical with actual ones. In this case, it can be known that l_2 and l_3 are allowed to be removed since they cannot affect the estimation process at all.

Thus, remaining gains in (10), besides l_2=l_3=0 and l_a=1, are set by proper pole-zero placement for $H_{\omega T}(s)$. For example, if one pole is placed on the real axis, i.e., $-p_1$, and two poles are on the complex plane, i.e., $-\zeta\omega_n \pm j\omega_n\sqrt{1-\zeta^2}$, gains are determined by (13) and the result is shown in (14).

$$\begin{aligned} &s^3+\left(\frac{\hat{B}_m}{\hat{J}_m}+l_b+l_1\right)s^2+\left(l_1\frac{\hat{B}_m}{\hat{J}_m}+l_c'+l_1l_b\right)s+l_1l_c' \\ &=(s-p_1)\cdot\left(s^2+2\zeta\omega_n s+\omega_n^2\right) \end{aligned} \quad (13)$$

$$\begin{aligned} &l_1=-p_1 \ \ or \ \ l_1=\omega_n\left(\zeta\pm\sqrt{(\zeta^2-1)}\right), \\ &l_b=-p_1+2\zeta\omega_n-\frac{\hat{B}_m}{\hat{J}_m}-l_1, \\ &l_c'=-2p_1\zeta\omega_n+\omega_n^2-l_1\frac{\hat{B}_m}{\hat{J}_m}-l_1l_b. \end{aligned} \quad (14)$$

If l_1 = -p_1 is selected, then the zero in $H_{\omega T}(s)$ can be canceled out and $H_{\omega T}(s)$ is simplified as (15).

$$H_{\omega T}(s)=\frac{P}{2\hat{J}_m}\cdot\frac{s}{s^2+2\zeta\omega_n s+\omega_n^2}. \quad (15)$$

By this procedure, robust estimation performance can be achieved and design process is simplified as well.

C. *Auxiliary speed estimator*

As mentioned above, although the response of $\hat{\theta}_r$ to ΔT can be much enhanced by setting l_a=1, that of $\hat{\omega}_r$ is still affected by it. Even if the increased gains would naturally reduce the effects, gains cannot be increased above certain limit since the estimated values by estimator become more sensitive to high-frequency noise. Therefore, in this paper, apart from the position and speed estimator introduced in previous section, an auxiliary speed estimator is proposed as shown in Fig. 4. The original estimator in Fig. 3 is changed to Fig. 4(b) with modifying the input stage. Modified estimator would operate combined with the auxiliary estimator in Fig. 4(a). In Fig. 4(a), l_i' is defined as $-Pl_i/2\hat{J}_m$. In the additional estimator, only the speed is estimated based on the state equation in (16).

$$\frac{d}{dt}\begin{bmatrix}\hat{\omega}_r\\ \hat{T}_L\end{bmatrix}=\begin{bmatrix}-\frac{\hat{B}}{\hat{J}_m} & -\frac{P}{2\hat{J}_m}\\ 0 & 0\end{bmatrix}\begin{bmatrix}\hat{\omega}_r\\ \hat{T}_L\end{bmatrix}+\begin{bmatrix}\frac{P}{2\hat{J}_m}\\ 0\end{bmatrix}T_e+\begin{bmatrix}l_p\\ l_i\end{bmatrix}\tilde{\omega}_{r,est}. \quad (16)$$

$$\begin{aligned} \hat{\theta}_r &= H_{\theta\theta}(s)\theta_r+H_{\theta\omega}(s)\omega_r+H_{\theta T}(s)\Delta T \\ \hat{\omega}_r &= H_{\omega\theta}(s)\theta_r+H_{\omega\omega}(s)\omega_r+H_{\omega T}(s)\Delta T \end{aligned}, \quad (11)$$

$$H_{\theta\theta}(s)=\frac{(1-l_a)(l_2s+l_3')+l_1s^2+\left(\frac{\hat{B}_m}{\hat{J}_m}l_1+l_1l_b\right)s+l_1l_c'}{(1-l_a)(l_2s+l_3')+s^3+\left(\frac{\hat{B}_m}{\hat{J}_m}+l_b+l_1\right)s^2+\left(\frac{\hat{B}_m}{\hat{J}_m}l_1+l_1l_b+l_c'\right)s+l_1l_c'},\quad H_{\theta\omega}(s)=\frac{(1-l_a)\left\{l_bs+l_c'+\frac{J_m}{\hat{J}_m}\left(s^2+\frac{B_m}{J_m}s\right)\right\}+l_a\left(s^2+\left(\frac{\hat{B}_m}{\hat{J}_m}+l_b\right)s+l_c'\right)}{(1-l_a)(l_2s+l_3')+s^3+\left(\frac{\hat{B}_m}{\hat{J}_m}+l_b+l_1\right)s^2+\left(\frac{\hat{B}_m}{\hat{J}_m}l_1+l_1l_b+l_c'\right)s+l_1l_c'},$$

where $H_{\omega\theta}(s)=\frac{s(l_2s+l_3')}{s^3+\left(\frac{\hat{B}_m}{\hat{J}_m}+l_b+l_1\right)s^2+\left(l_1\frac{\hat{B}_m}{\hat{J}_m}+l_c'+l_1l_b\right)s+l_1l_c'+(l_2s+l_3')(1-l_a)}$, $H_{\omega\omega}(s)=\frac{\frac{J_m}{\hat{J}_m}s^3+\left(\frac{B_m}{\hat{J}_m}+l_b+l_1\frac{J_m}{\hat{J}_m}\right)s^2+\left(l_1l_b+l_c'+l_1\frac{B_m}{\hat{J}_m}\right)s+l_1l_c'-l_a(l_2s+l_3')}{s^3+\left(\frac{\hat{B}_m}{\hat{J}_m}+l_b+l_1\right)s^2+\left(l_1\frac{\hat{B}_m}{\hat{J}_m}+l_c'+l_1l_b\right)s+l_1l_c'+(l_2s+l_3')(1-l_a)}$,

$H_{\theta T}(s)=\frac{\frac{P}{2\hat{J}_m}(1-l_a)s}{(1-l_a)(l_2s+l_3')+s^3+\left(\frac{\hat{B}_m}{\hat{J}_m}+l_b+l_1\right)s^2+\left(\frac{\hat{B}_m}{\hat{J}_m}l_1+l_1l_b+l_c'\right)s+l_1l_c'}$, $H_{\omega T}(s)=\frac{\frac{P}{2\hat{J}_m}s(s+l_1)}{s^3+\left(\frac{\hat{B}_m}{\hat{J}_m}+l_b+l_1\right)s^2+\left(l_1\frac{\hat{B}_m}{\hat{J}_m}+l_c'+l_1l_b\right)s+l_1l_c'+(l_2s+l_3')(1-l_a)}$.

In (16), with the assumption of $\tilde{\omega}_{r,est} = \tilde{\omega}_r$, l_p and l_i can be determined by the transfer functions in (17).

$$\hat{\omega}_r = \frac{\frac{J_m}{\hat{J}_m}s^2 + \left(l_p + \frac{B_m}{\hat{J}_m}\right)s + l_i'}{s^2 + 2\zeta_{aux}\omega_{n,aux}s + \omega_{n,aux}^2}\omega_r + \frac{\frac{P}{2\hat{J}_m}s}{s^2 + 2\zeta_{aux}\omega_{n,aux}s + \omega_{n,aux}^2}\Delta T \quad (17)$$

where $s^2 + 2\zeta_{aux}\omega_{n,aux}s + \omega_{n,aux}^2 = s^2 + \left(l_p + \frac{\hat{B}_m}{\hat{J}_m}\right)s + l_i'$.

From the comparison between (15) and (17), it can be known that their forms are the same. Therefore, for the auxiliary speed estimator to be effective, it should have higher bandwidth than original one in (15) to reduce the effects of ΔT on $\hat{\omega}_r$. In this way, minimizing the effects of noise on $\hat{\theta}_r$, more robust speed-estimating performance can be achieved.

On the other hand, the speed error input to the original estimator in Fig. 4(b) should be determined. For the design of the original estimator to be still valid, this value should have the difference between the actual speed, ω_r, and the unused state variable, $\hat{\omega}_r'$, in Fig. 4(b). For calculation of $\omega_r - \hat{\omega}_r'$, indirect calculation method can be used as shown in (18).

$$\begin{aligned}\tilde{\omega}_r' &= \omega_r - \hat{\omega}_r' = (\omega_r - \hat{\omega}_r) - (\hat{\omega}_r' - \hat{\omega}_r) \\ &\approx \tilde{\omega}_{r,est} - (\hat{\omega}_r' - \hat{\omega}_r)\end{aligned} \quad (18)$$

From (18), it can be known that the input to the original estimator can be determined using $\tilde{\omega}_{r,est}$ from (9) and the state variables, $\hat{\omega}_r'$ and $\hat{\omega}_r$. Therefore, the auxiliary speed estimator can be superimposed to the original estimator without any effect on characteristics of each estimator.

TABLE I. PARAMETERS OF IPMSM

IPMSM Parameters	Value
Rated power	300 W
Rated current	2.85 A_{rms}
Pole number	6
Back EMF constant (λ_f)	0.064 V·s
Winding resistance	0.76 Ω
Synchronous inductances	L_{ds}: 7.15 mH, L_{qs}: 10.6 mH

IV. EXPERIMENTAL RESULTS

For verification of the proposed methods, several experiments are designed. In experimental system, M-G set is made up to emulate the loads. Before the experiments, voltage distortion characteristics and parameters were extracted. Since the error between the reference and applied voltage is a cause for position error, it should be properly compensated in model-based sensorless control. In implementation, compensation voltages in Fig. 5 are superimposed to the output voltages of the controller according to the phase currents. In addition, parameters of the test motor are specified in Table I. Regarding L_{qs} in test motor, it is almost constant if i_{qs}^r is in the range of 0.3 ~ 0.7 p.u.. Therefore, for convenience, experiments are designed in this range.

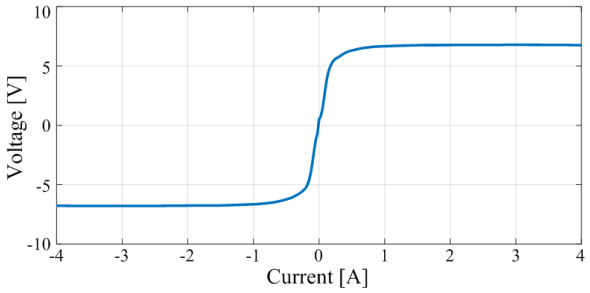

Fig. 5. Distortion voltage according to the phase current.

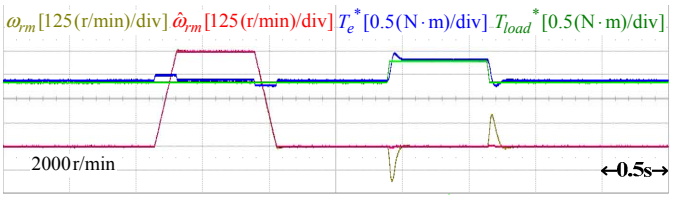

(a) Variation of ω_{rm}, $\hat{\omega}_{rm}$, T_e^* and T_{load}^*

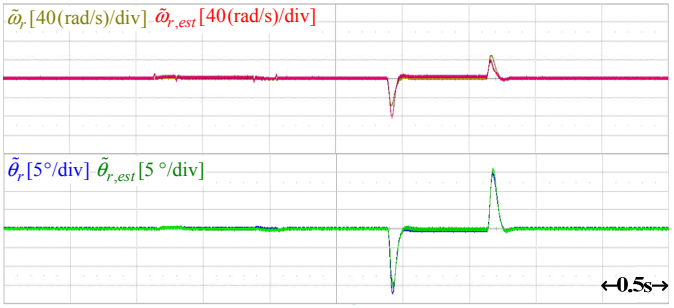

(b) Comparison between the actual and estimated values

Fig. 6. Verification of the proposed estimation method for $\tilde{\theta}_{r,est}$ and $\tilde{\omega}_{r,est}$.

Following experimental results show that the estimated values, i.e., $\tilde{\theta}_{r,est}$ and $\tilde{\omega}_{r,est}$, well match to actual values and sensorless control performance can be conspicuously enhanced by the proposed methods in both of the current and speed control modes.

A. Verification of estimated position and speed error

The proposed estimation methods in (9) are verified by comparing $\tilde{\theta}_{r,est}$ and $\tilde{\omega}_{r,est}$ with the actual errors, i.e., $\tilde{\theta}_r$ and $\tilde{\omega}_r$, from position sensor. In this experiment, the test motor is operated in speed control mode ($\omega_{rm}^* = 2000$ r/min) without the position sensor which is used only for observing $\tilde{\theta}_r$ and $\tilde{\omega}_r$. In sensorless control, $\tilde{\theta}_{r,est}$ is estimated by (5) and it is used as an input to the estimator in Fig. 2.

Fig. 6 shows the comparison results between the actual and estimated error. As shown in Fig. 6(a), even in the highly dynamic operation including speed (3000 r/min/s) and load torque variation (0.3 → 0.7 → 0.3 p.u., by 20 p.u. /s), it can be noted in Fig. 6(b) that $\tilde{\theta}_{r,est}$ and $\tilde{\omega}_{r,est}$ are identical with actual ones. Therefore, it can be concluded that the assumptions in (7) and (9) are reasonable and the estimated values can be used as an input to the proposed estimators in Fig. 3 and Fig. 4.

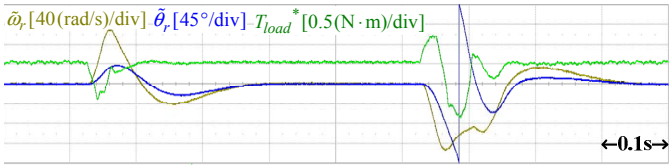

(a) Conventional method

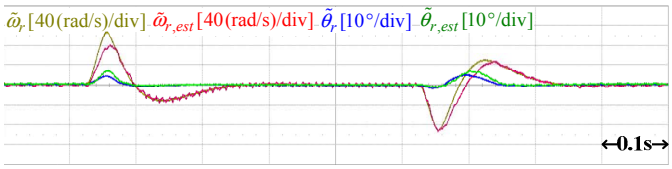

(b) Proposed method without auxiliary speed estimator

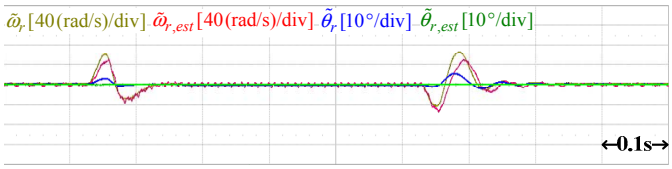

(c) Proposed method with auxiliary speed estimator

Fig. 7. Position and Speed error in speed variation (500 ↔ 1000 r/min).

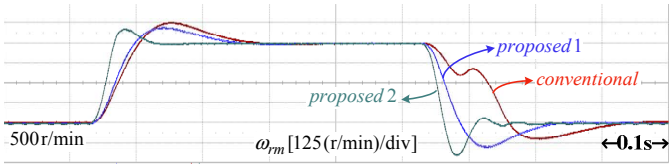

Fig. 8. Estimated speeds by each method.

B. *Abrupt speed variation (20,000 r/min /s) in current control mode*

In Fig. 7-8, experimental results are presented when the motor is in current control mode ($i_{qs}^{r*} = 0.5$ p.u.) and the load machine regulates the rotating speed in speed control mode. In Fig. 7, rotating speed is varied by load machine from 500 r/min to 1,000 r/min, and back to 500 r/min again with the rate of 20,000 r/min /s. In the experiments, three different methods are compared. One is the aforementioned conventional method using (5) and the estimator in Fig. 2, whose result is shown in Fig. 7(a). The proposed methods are used in Fig. 7(b)-(c) where the difference is whether the auxiliary speed estimator in Fig. 4 is added or not. Even if the pole-placement for estimators is equally set as $p_1 = -8$Hz, $\omega_n = 4$Hz, $\zeta = 0.7$ and $\omega_{n,aux} = 10$Hz, $\zeta_{aux} = 0.7$ for the auxiliary estimator, it can be noticed that the performance in Fig. 7(c) is remarkable compared to other methods, especially, in the first transient. In Fig. 7(a), the position error exceeds even the stability limit, i.e., 90°, and it can be noted that the applied load torque is abruptly changed into reversed way. Meanwhile, in Fig. 7(b)-(c), the maximum position error is less than 5° during the transient. Additionally, in Fig. 7(c) which employs the auxiliary speed estimator, the maximum speed error has been reduced by 30% compared to Fig. 7(b) as well as the response time is decreased to less than 50% in the first transient. Fig. 8 shows the estimated speeds by each method. As shown in the figure, even if the maximum overshoot is similar to each other, it can be noted that the proposed method with auxiliary estimator which is marked as '*proposed 2*' has much faster response than any others.

In Fig. 9, experimental results are presented when the operating speed is varied from 2,000 r/min to 2,500 r/min, and

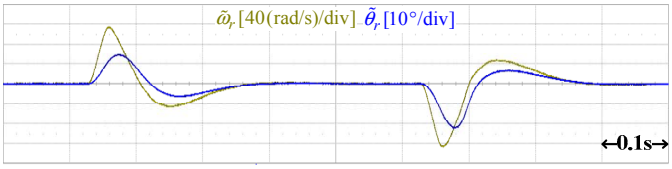

(a) Conventional method

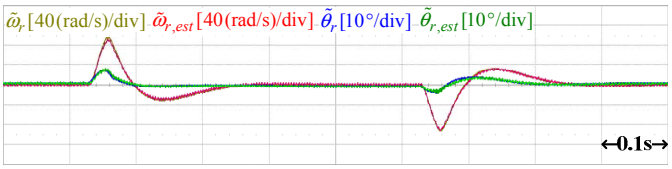

(b) Proposed method without auxiliary speed estimator

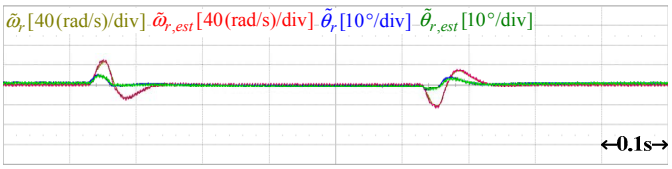

(c) Proposed method with auxiliary speed estimator

Fig. 9. Position and Speed error in speed variation (2000 ↔ 2500 r/min).

back to 2,000 r/min with the rate of 20,000 r/min /s. In this condition, it can be seen from Fig. 9(a) that the conventional method can be operated in stable. However, its resulting position and speed error reach 20° and 120 rad/s, respectively. Meanwhile, in Fig. 9(b), it can be seen that while the resulting speed error is similar with the conventional method, the maximum position error is conspicuously reduced by more than 50%. It is because that the resulting speed error can be reflected in the position estimation process. In Fig. 9(c), the proposed method with the auxiliary estimator shows the best performance in view of the magnitude of errors and the response time. The position and speed errors are reduced by more than 60% and the response time is also decreased to 50%. Pole-placement for estimators is set as same with the lower speed case in Fig. 7-8.

C. *Abrupt load torque disturbance (20 p.u. /s) during speed control mode*

In these experiments, robustness is tested under the speed control mode. In experiments, abrupt load torque, T_{load}, is rapidly applied from 0.3 p.u. to 0.7 p.u., and back to 0.3 p.u. again with the rate of 20 p.u. / s. Operating speed is regulated by the test motor as 500 r/min and 2000 r/min in sequence.

Firstly, variation of T_{load} is shown in Fig. 11 together with the estimated speeds by each method. As shown in Fig. 11, in case of the conventional method, it can be noted that it yields to the external disturbance and fails to maintain the speed. Therefore, the errors only for the proposed methods are presented in Fig. 10. In Fig. 10, it can be noted that while the maximum speed error of the first transient in Fig. 10(a) is 110 rad/s, the error in Fig. 10(b) is 50 rad/s, which is only 45% of the first case. Similarly, in the second transient, the speed error of the latter is just a half of the former even if the response is little oscillatory. Moreover, their maximum position error is also reduced. Resulting maximum error is 30° in Fig. 10(a). However, it can be seen from Fig. 10(b) that the maximum value has been reduced to 15°.

Speed control performance of the proposed method using auxiliary estimator is also superior to other methods. As shown

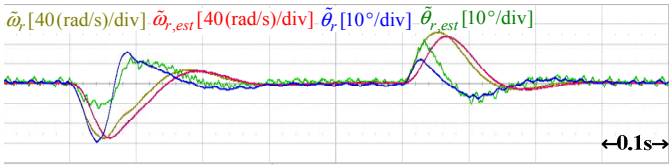

(a) Proposed method without auxiliary speed estimator

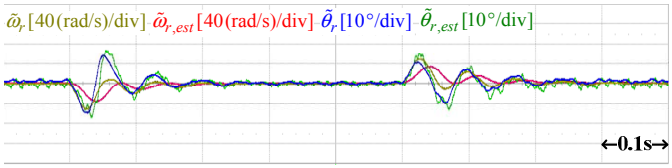

(b) Proposed method with auxiliary speed estimator

Fig. 10. Position and Speed error in load torque variation (0.3 ↔ 0.7 p.u.).

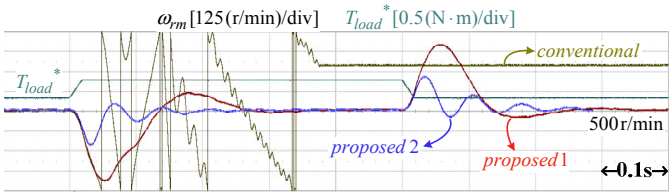

Fig. 11. Estimated speeds by each method in load torque variation (500 r/min).

in Fig. 11, '*proposed 2*' shows the more robust response and faster reference tracking ability. In 500 r/min experiments, pole-placement for estimators is set as $p_1 = -20\text{Hz}$, $\omega_n = 4\text{Hz}$, $\zeta = 0.7$ and $\omega_{n,aux} = 7\text{Hz}$, $\zeta_{aux} = 1.8$.

Fig. 12 and Fig. 13 show speed control performances when the reference speed is 2000 r/min. In this case, the difference of the performance is clearer than 500 r/min condition since the high-frequency noise components can be filtered out by rotating inertia. In Fig. 12 (a), while the resulting position error reach 20º by the conventional method, it is less than 5º in proposed methods. Also, in Fig. 12(c) and Fig. 13, similar with the previous results in Fig. 10, resulting speed error in the proposed method using auxiliary estimator has been reduced by 50% from other methods with the reduced oscillatory components. In 2000 r/min experiments, pole-placement is set as $p_1 = -20\text{Hz}$, $\omega_n = 6\text{Hz}$, $\zeta = 0.7$ and $\omega_{n,aux} = 10\text{Hz}$, $\zeta_{aux} = 1.6$.

From the experimental results, it can be concluded that the robustness of the sensorless control has been much enhanced and current and speed control performances also have been improved by the proposed methods.

V. Conclusion

In this paper, new estimation methods for the position and speed errors and compatible position and speed estimators were proposed. In the proposed methods, the speed error as well as the position error was extracted by segregating the actual speed term in voltage equation into the estimated and error terms. Also, the position and speed estimator using the estimated errors has been proposed and proper gain setting method was also guided. In this way, the position error can be nullified even in the transient by disturbance torque. Additionally, the auxiliary speed estimator was proposed for higher robustness of the estimated speed. All proposed methods were verified by experiments and experimental results showed the effectiveness

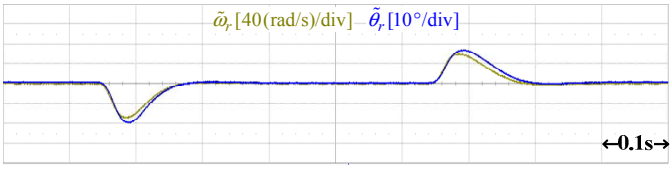

(a) Conventional method

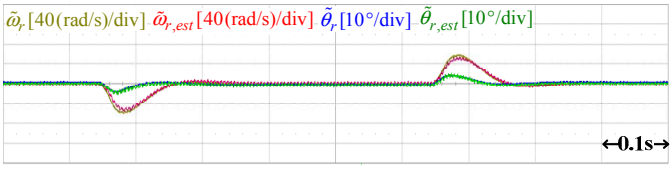

(b) Proposed method without auxiliary speed estimator

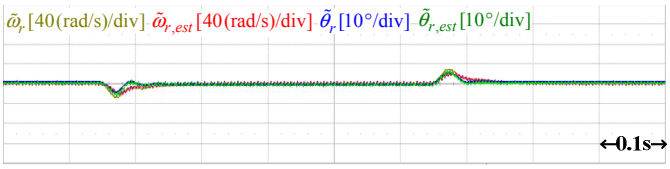

(c) Proposed method with auxiliary speed estimator

Fig. 12. Position and Speed error in load torque variation (0.3 ↔ 0.7 p.u.).

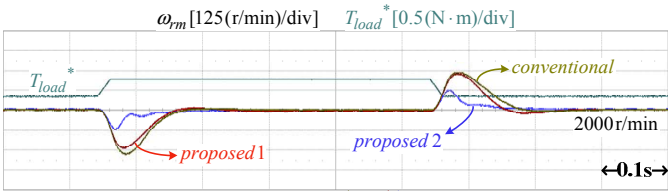

Fig. 13. Estimated speeds by each method in load torque variation (2000 r/min).

of the proposed methods under severe speed and load torque transient conditions. With the proposed methods, position error has been conspicuously reduced by 60% at speed transient and by 70% at load torque transient in high speed region.

References

[1] J.-H. Jang, J.-I. Ha, M. Ohto, K. Ide, and S.-K. Sul, "Analysis of permanent-magnet machine for sensorless control based on high-frequency signal injection," *IEEE Trans. Ind. Appl.*, vol. 40, pp. 1595-1604, Nov/Dec. 2004.

[2] D. Kim, Y.-C. Kwon, S.-K. Sul, J.-H. Kim, and R.-S. Yu, "Suppression of Injection Voltage Disturbance for High-Frequency Square-Wave Injection Sensorless Drive With Regulation of Induced High-Frequency Current Ripple," *IEEE Trans. Ind. Appl.*, vol. 52, pp. 302-312, Jan/Feb. 2016.

[3] Y. Li, Z. Q. Zhu, D. Howe, C. M. Bingham, and D. A. Stone, "Improved Rotor-Position Estimation by Signal Injection in Brushless AC Motors, Accounting for Cross-Coupling Magnetic Saturation," *IEEE Trans. Ind. Appl.*, vol. 45, pp. 1843-1850, Sep./Oct. 2009.

[4] Y.-D. Yoon, S.-K. Sul, S. Morimoto, and K. Ide, "High-Bandwidth Sensorless Algorithm for AC Machines Based on Square-Wave-Type Voltage Injection," *IEEE Trans. Ind. Appl.*, vol. 47, pp. 1361-1370, May./Jun. 2011.

[5] S. Kim, J.-I. Ha, and S.-K. Sul, "PWM Switching Frequency Signal Injection Sensorless Method in IPMSM," *IEEE Trans. Ind. Appl.*, vol. 48, pp. 1576-1587, Sep./Oct. 2012.

[6] Y. Inoue, K. Yamada, S. Morimoto, and M. Sanada, "Effectiveness of Voltage Error Compensation and Parameter Identification for Model-Based Sensorless Control of IPMSM," *IEEE Trans. Ind. Appl.*, vol. 45, pp. 213-221, Jan./Feb. 2009.

[7] K.-W. Lee and J.-I. Ha, "Evaluation of Back-EMF Estimators for Sensorless Control of Permanent Magnet Synchronous Motors," *J. Power Electron.*, vol. 12, pp. 604-614, Jul. 2012.

[8] Y. Lee, Y.-C. Kwon, and S.-K. Sul, "Comparison of Rotor Position Estimation Performance in Fundamental-Model-Based Sensorless Control of PMSM," in *Proc. IEEE ECCE 2015*, pp. 5624–5633, Sep. 2015.

[9] S. Morimoto, K. Kawamoto, M. Sanada, and Y. Takeda, "Sensorless control strategy for salient-pole PMSM based on extended EMF in rotating reference frame," *IEEE Trans. Ind. Appl.*, vol. 38, pp. 1054-1061, Jul./Aug. 2002.

[10] Z. Chen, M. Tomita, S. Doki, and S. Okuma, "An Extended Electromotive Force Model for Sensorless Control of Interior Permanent-Magnet Synchronous Motors," *IEEE Trans. Ind. Electron.*, vol. 50, pp. 288-295, Apr. 2003.

[11] K. Lu, X. Lei, and F. Blaabjerg, "Artificial Inductance Concept to Compensate Nonlinear Inductance Effects in the Back EMF-Based Sensorless Control Method for PMSM," *IEEE Trans. Energy Convers.*, vol. 28, pp. 593-600, Sep. 2013.

[12] H. Kim, M. C. Harke, and R. D. Lorenz, "Sensorless control of interior permanent-magnet machine drives with zero-phase lag position estimation," *IEEE Trans. Ind. Appl.*, vol. 39, pp. 1726-1733, Nov./Dec. 2003.

[13] T. Senjyu, T. Shingaki, and K. Uezato, "Sensorless vector control of synchronous reluctance motors with disturbance torque observer," *IEEE Trans. Ind. Electron.*, vol. 48, pp. 402-407, Apr. 2001.

[14] N. Matsui, T. Takeshita, and K. Yasuda, "A new sensorless drive of brushless DC motor," in *Proc. IEEE IECON 1992*, pp. 430-435, Nov. 1992.

[15] N. Matsui, "Sensorless PM brushless DC motor drives," *IEEE Trans. Ind. Appl.*, vol. 43, pp. 300-308, Apr. 1996.